IOP Publishing Journal of Physics: Condensed Matter
J. Phys.: Condens. Matter **27** (2015) 134203 (8pp) doi:10.1088/0953-8984/27/13/134203

Searching for new TiO_2 crystal phases with better photoactivity

Cheng Shang, Wei-Na Zhao and Zhi-Pan Liu

Key Laboratory of Computational Physical Science (Ministry of Education), Shanghai Key Laboratory of Molecular Catalysis and Innovative Materials, Department of Chemistry, Fudan University, Shanghai 200433, China

E-mail: zpliu@fudan.edu.cn

Received 14 May 2014, revised 11 June 2014
Accepted for publication 23 June 2014
Published 13 March 2015

Abstract

Using the recently developed stochastic surface walking global optimization method, this work explores the potential energy surface of TiO_2 crystals aiming to search for likely phases with higher photocatalytic activity. Five new phases of TiO_2 are identified and the lowest energy phase transition pathways connecting to the most abundant phases (rutile and anatase) are determined. Theory shows that a high-pressure phase, α-PbO_2-like form (TiO_2II) acts as the key intermediate in between rutile and anatase. The phase transition of anatase to rutile belongs to the diffusionless Martensitic phase transition, occurring through a set of habit planes, rutile(101)//TiO_2II(001), and TiO_2II(100)//anatase(112). With regard to the photocatalytic activity, three pure phases (#110, pyrite and fluorite) are found to possess the band gap narrower than rutile, but they are unstable at the low-pressure condition. Instead, a mixed anatase-TiO_2II phase is found to have good stability and narrower band gap than both parent phases. Because of the phase separation, the mixed phase is also expected to improve the photocatalytic performance by reducing the probability of the electron-hole pair recombination.

Keywords: photocatalysis, titania phases, global optimization

(Some figures may appear in colour only in the online journal)

1. Introduction

Titania is an important material with a wide application in technology. Its photoactivity, in particular, has attracted much attention, not least because of the high stability under photon-radiation, but also adequate efficiency for water oxidation [1–9]. To date, the nature of the photoactive sites of titania polymorphs at the solid-liquid interface remains largely elusive. There are a number of stable phases for TiO_2 in nature, including the well-known minerals rutile, anatase, and brookite and two high-pressure forms, a monoclinic baddeleyite-like form (MI phase [10]) and an orthorhombic α-PbO_2-like form (TiO_2II phase [11]). It has been a long-standing puzzle that single crystal rutile and anatase have poorer photoactivity compared to polymorphs, which were attributed to more or different sites in polymorphs that commonly contain a mixture of different phases, often rutile and anatase [12–16]. Here, a recently developed global optimization method is utilized for exploring TiO_2 crystal potential energy surface (PES) aiming to identify interesting new phases and their connection to the common TiO_2 phases, which might be of potential significance for the design of photocatalysts.

Owing to the presence of multiple stable phases, the solid-to-solid phase transition has been exploited commonly in the synthesis of TiO_2 nanostructures [17]. Under ambient conditions, the metastable anatase and brookite phases convert to rutile upon heating for large particles, while the rutile phase reverts to anatase phase for small nanoparticles due to the lower surface energy of anatase. This phase transition provides profound influences on the physiochemical properties, including photoactivity. Recently, Ohno *et al* [13]. and Bickley *et al* [12]. found a clear synergistic effect for the photocatalytic activity of P-25 TiO_2 powder (anatase to rutile ratio is about 4:1). Similarly, Zhang *et al* [14]. pointed out that the presence of the phase junction between anatase and rutile can greatly enhance the photocatalytic activity by up to four times

as evidenced by Raman spectroscopy and high-resolution TEM. Since these experimental evidences indicate the importance of phase transition, in particular for the photocatalytic mechanism on the composite, the atomic structure of the phase junction and the transition mechanism have triggered enormous interests in the last decades. Through well-controlled synthesis, Penn, Banfield, and coworkers have observed that the anatase {112} twin junction initiates the phase transformation [18, 19], which has been confirmed in recent molecular dynamics studies [20] and light-induced phase transition from anatase to rutile [21]. In general, the mechanism of rutile to anatase phase transition has been much discussed in the literature, the phase transition between the other phases of TiO_2 are not well documented.

Inspired by these experimental findings, one may conceive that better photocatalysts are likely present constituted by unknown phases of TiO_2, either with single component and multiple components (mixed phases). For this purpose, theoretical methods might be an ideal explorative tool to identify the new phases interesting as photocatalysts. In this work, we utilized the recently developed global optimization method, namely the stochastic surface walking (SSW) method [22, 23], for exploring the phases of TiO_2 crystal and sampling transition pathways between them. Several new TiO_2 phases are identified, and according to the phase transition pathway the mixed phase material is also constructed, which shows unexpected electronic structure. Their potential as photocatalysts is discussed in the context of experimental findings.

2. Calculation Method

2.1. SSW-crystal method for PES exploration

The recently developed SSW method [22, 23] with appropriate modifications to include the lattice degrees of freedom (SSW-crystal) is utilized to explore the PES of TiO_2 crystal. The SSW algorithm features an unbiased PES exploration ability using the second derivative information. The method originates from the bias-potential driven constrained Broyden dimer (BP-CBD) method for transition state (TS) searching developed in the group [22, 24], in which the barrier of reaction is surmounted by adding consecutively Gaussian bias potentials and the reaction coordinate (the direction where Gaussian is added) is refined continuously using the biased constrained Broyden dimer (biased-CBD) method. Different from the BP-CBD method, each SSW step (from one minimum to another) will choose a random direction and perturb structure along the direction that is always refined using the biased-CBD method. At the end of the SSW step, a structure selection module, e.g. in Metropolis Monte-Carlo scheme, is applied to accept/refuse the new minimum. The detail of the methodology can be found in a previous aticle [22, 23]. The SSW parameters utilized in this work is as follows: the Gaussian width is 0.6 Å; the number of Gaussian is 10.

For the pathway sampling between TiO_2 phases, first, we start from one single phase, the initial state (IS) phase, and utilize the (SSW-crystal) method to explore all the likely phases nearby. The structure selection module is utilized to decide whether to accept/refuse once a new minimum is reached. If a new phase different from the IS phase is identified, we record/output the IS structure and the final state (FS) phase (a new phase) of the current SSW step. Then, the program will return back to the IS by rejecting the new minimum to continue the phase exploration. On the other hand, if the new minimum identified is the same as the starting phase (e.g. the same symmetry but a permutation isomer with varied lattice), the program will accept the new isomeric structure and continue the structure exploration. Second, we repeat the whole procedure until a certain number of IS/FS pairs are collected, typically a few hundred. The maximum number of the minima nearby visited is set as 10^4 in this work. Third, we utilize the variable-cell double-ended surface walking method (variable-cell DESW [25]) to identify the TSs explicitly for all the IS/FS pairs [24, 26], which is confirmed using numerical frequency analysis. The low energy pathways are thus determined according to the located TSs using the calculated barrier being the energy difference between the TS and the IS. It should be mentioned that for every interested phase of TiO_2, we need to repeat the above procedure to obtain the connectivity of the phase until the whole reaction network containing all the important phases is completed.

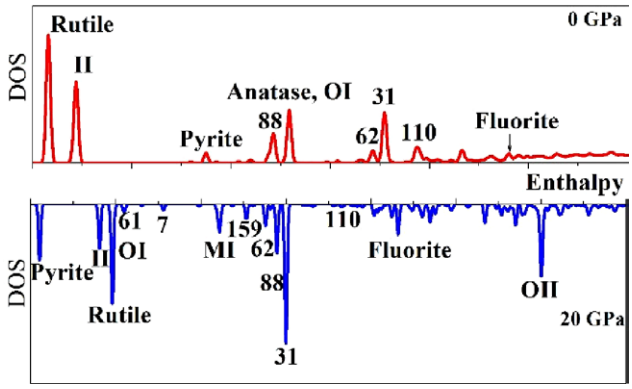

Figure 1. The probability density, g(E) of minima for TiO_2 (using classical MA potential) at zero and 20 GPa pressure using SSW-crystal method in combination with Wang–Landau algorithm; Symmetry symbol is labeled.

2.2. Calculation details for TiO_2 system

Both the classical potential using Matsui–Akaogi (MA) interatomic potential [27] and density functional theory (DFT) calculations have been utilized for TiO_2 systems. The classical potential calculations are mainly for sampling exhaustively the likely phase transition pathways and the latter are to refine and obtain the accurate energetics for the lowest energy pathways and water splitting kinetics. The MA potential has been demonstrated to describe reasonably well the phase diagram of TiO_2 at different pressure conditions [27, 28]. It should be mentioned that due to the huge amount of possible reaction pathways between different phases, the classical simulations are essential for the initial screening of the reaction pathways (up to 10^4 pathways sampled for each phase), and they provide a low energy database of the reaction coordinates

Table 1. DFT calculated bulk energy per TiO_2 unit (E/eV), the relative band gap (ΔE_g/eV), the coordination number of Ti (C_{Ti}) and the optimized lattice parameters (length in Å) for the TiO_2 phases identified from SSW-crystal.

Name	E*	ΔE_g*	a	b	c	α °	β °	γ°	Space Group	C_{Ti}
Anatase [46]	-0.099	0.36	3.80	3.80	9.78	90	90	90	$I4_1/amd$ (#141)	6
Brookite [47]	-0.054	0.52	9.28	5.52	5.19	90	90	90	*Pbac* (#61)	6
II [48]	-0.018	0.79	4.59	5.60	4.93	90	90	90	*Pbcn* (#60)	6
Rutile [49]	0.000	0.00	4.66	4.66	2.97	90	90	90	$P4_2/mnm$ (#136)	6
Lepidocrocite [40]	0.072	1.13	3.74	3.03	11.96	90	90	90	*Pmmn* (#59)	6
MI [50]	0.093	0.55	4.88	4.92	5.15	90	100.59	90	$P2_1/c$ (#14)	7
#61	0.144	0.19	9.59	4.90	5.05	90	90	90	*Pbca* (#61)	7
#7	0.207	0.34	9.53	4.97	4.96	90	95.71	90	*Pc*(#7)	7
OI [28]	0.255	0.31	9.45	4.99	4.86	90	90	90	*Pbca* (#61)	7
#88	0.270	0.67	4.77	4.77	10.96	90	90	90	$I4_1/a$ (#88)	6
#110	0.513	-0.29	4.91	4.91	9.76	90	90	90	$I4_1cd$ (#110)	6
#159	0.534	0.51	6.86	6.86	5.61	90	90	120	$P31c$ (#159)	7
Pyrite [39]	0.648	-0.12	4.90	4.90	4.90	90	90	90	$Pa\bar{3}$ (#205)	6
Fluorite [51]	0.810	-0.71	4.84	4.84	4.84	90	90	90	$Fm\bar{3}m$ (#225)	8

*The energy and the band gap of rutile is set as reference.

(IS/FS pairs) for the phase transition; based on this, the first principles calculations can then be performed to compare the energetics between different pathways.

The DFT calculations of bulk TiO_2 phases are performed using the CASTEP package [29] with plane wave basis set [30] and ultrasoft pseudopotentials [31]. The generalized gradient approximation method, known as GGA-PBE was used as the exchange–correlation functional [32, 33]. A kinetic cutoff energy of 340 eV was used and Monkhorst-Pack k-point sampling with approximately 0.04 $Å^{-1}$ spacing was utilized for all of the calculations. The DFT calculations on the phase transition pathways are performed using the SIESTA package [34] with optimized numerical double-ζ polarization basis set [35, 36] at the GGA-PBE exchange-correlation functional level. The energy cutoff for the real space grid used to represent the density was set as 150 Ry. An energy shift of 0.01 eV was used to determine the orbital-confining cutoff radii. For all the lattice studied, the **k**-point mesh utilized was Monkhorst–Pack (4 × 4 × 4) set, which is verified to be enough to obtain good energetics.

3. Results and discussion

3.1. TiO_2 phases from SSW-crystal/Wang–Landau method

Since our aim is to identify the interesting TiO_2 phases that might be of potential application in photocatalysis, we start our simulation with exploring the TiO_2 PES by combining SSW-crystal method with Wang–Landau (WL) flat histogram algorithm [22, 23, 37]. In the WL algorithm, the density of states (DOS) is generated by performing a set of random walks in energy space with a probability proportional to the reciprocal of the density of states. By modifying the estimated DOSs in a systematic way, a flat histogram over the allowed range of energy can be produced, and the DOSs will simultaneously converge to the true value. For exploring the phases of TiO_2 crystal, about 10^7 minima are visited by SSW to reach the flat histogram in Wang–Landau DOS. The Wang–Landau DOS is shown in figure 1 for TiO_2 crystal (24 atoms/cell) at 0 GPa and at 20 GPa. All the major phases identified with a relatively large DOS are labeled in figure 1. The other common phase, e.g. brookite, has also been identified but with very low DOS. We found that the SSW-crystal/WL method identifies all the major known phases of TiO_2 and also a number of new phases that have not been reported previously in literatures.

Rutile ($P4_2/mnm$, #136), TiO_2II (*Pbcn*, #60) and anatase phases ($I4_1/amd$, #141) have the largest DOS at zero pressure. By elevating to 20 GPa, the presence of TiO_2II increases together with the other known high-pressure phases, namely OI (*Pbca*, #61), MI ($P2_1/c$, #14), fluorite ($Fm\bar{3}m$, #225), OII (*Pnma*, #62) phases [38], and pyrite ($Pa\bar{3}$, #205). (Note that the MA potential tends to over-stabilize the pyrite phase [10, 28, 39]). The SSW-crystal also identifies several new phases with large DOSs, namely $I4_1/a$ (#88), *Pnam* (#62), $Pn2_1m$ (#31), $I4_1cd$ (#110), *Pbca* (#61), *Pc* (#7) and $P3_1c$ (#159), which, to the best our knowledge, were not discovered previously in experiments.

DFT calculations at zero pressure are then utilized to verify the stability of these phases, which confirms that #88, #110, #61, #7, #159 are stable phases at zero pressure, while #31 and #62 turn out to be a layered structure known as lepidocrocite typed structure [40] (*Pmmn,* #59) after structural optimization. The lattice parameters of the crystal structures optimized are listed in table 1 and the structures of them are shown in figure 2. Our calculated structures for the known phases are in good agreement with results from experiments and the previous theoretical works [39, 41–43]. It has been reported that the DFT calculations including the hybrid functionals predict wrongly the order of relative stability for anatase and rutile, although the energy difference is very small [39, 44, 45]. This is as also found in this article: anatase is 0.099 eV per TiO_2 unit more stable than rutile.

For the new phases, #110 and #88 contain only 6-coordinated Ti (Ti_{6c}) and 3-coordinated O (O_{3c}), similar to rutile, anatase, brookite, pyrite, and TiO_2II; #159, #61, and #7 have Ti_{7c}, and both O_{3c} and O_{4c} at the equivalent concentration, similar to the known phases at high pressures, such as OI, OII, and MI. It might be mentioned that the new phase #61 (Pbca,

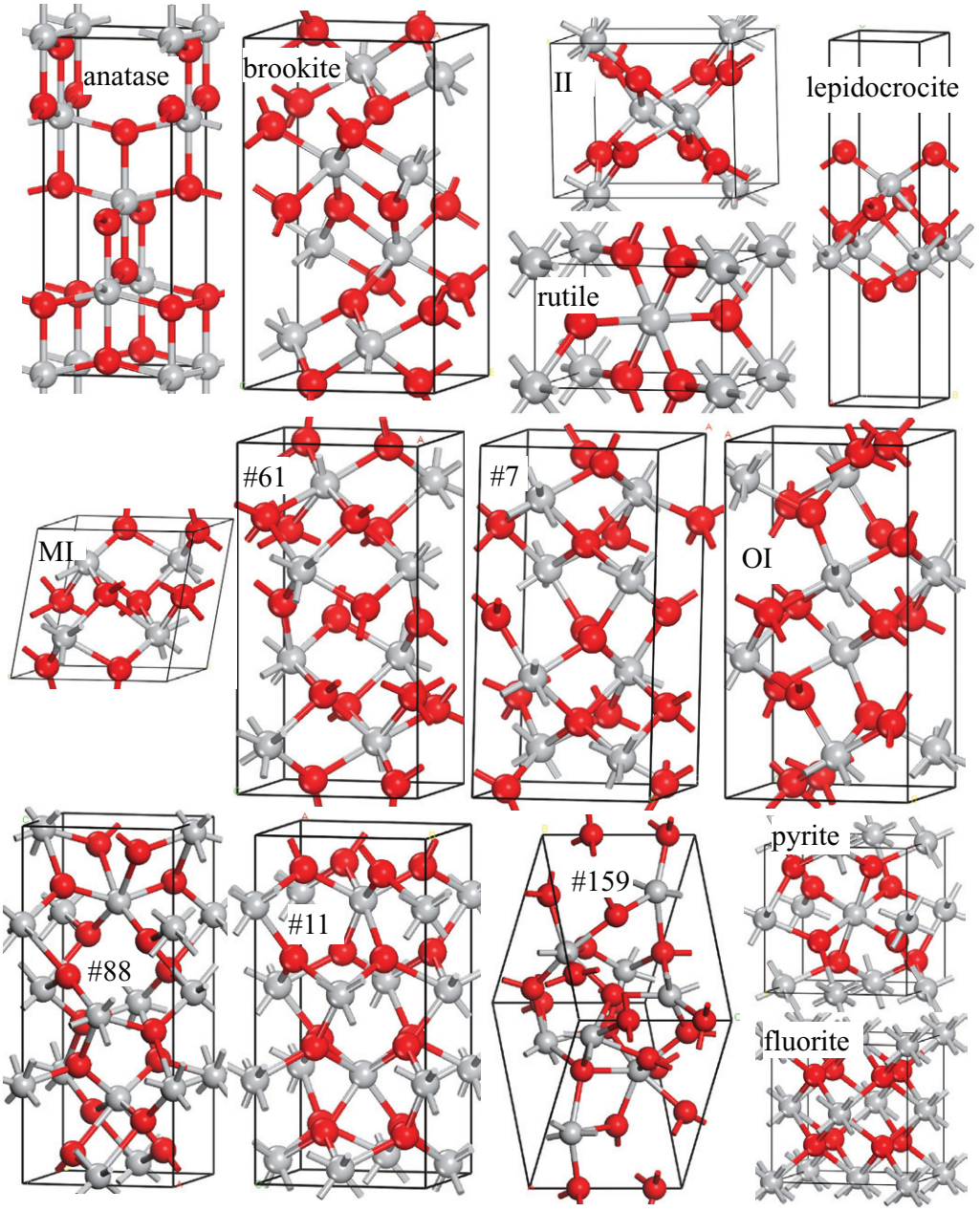

Figure 2. DFT optimized bulk phase structure identified from SSW-crystal global optimization. Gray and red spheres represent Ti and O atoms, respectively.

a=9.60; b=4.90; c=5.05 Å; $\alpha = \beta = \gamma = 90.0°$) is different from the high-pressure OI phase despite the same symmetry group. It is only 0.144 eV/(TiO_2) less stable than rutile at 0 GPa and 0.036 eV/(TiO_2) less stable than MI at 15 GPa.

3.2. Phase transition pathway between TiO_2 phases

With all the major minima of TiO_2 crystal gleaned from SSW-crystal method, we are at the position to sample the pathways that can link one particular phase to its nearby phases. This is essential for understanding the phase connectivity, where the lowest energy pathway between phases matters from kinetics. Due to the complexity of the PES, the pathway sampling was carried out using the classical MA potential with 12 atoms per cell (Ti_4O_8) to generate the database of possible pathways. For each sampling, i.e. starting from one particular phase, 10000 SSW steps were performed to collect the pathways (see Section 2 for calculation method). The DFT calculations were then utilized to examine a number of selected low energy pathways, from which the lowest energy reaction pathway is obtained. The DFT lowest energy pathway for the major phases is shown in figure 3. It should be mentioned that the size of the unit cell can limit the phase space of crystal and thus the barriers reported here should be considered to be the maximum limit for the phase transition. We expect that the connectivity relationship between the phases should be invariant with the increase of the unit cell, which is determined by the structure similarity of the phases.

Figure 3 shows that the lowest barrier transition channel leaves the rutile phase via two common high-pressure phases,

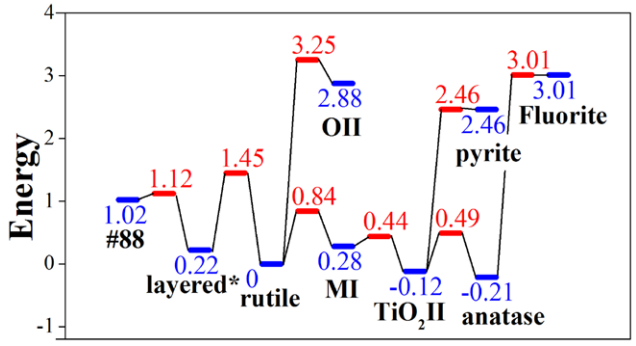

Figure 3. The DFT lowest energy connectivity map of the major phases at zero pressure. The energy unit is eV per Ti_4O_8 cell. The energy of rutile is set to zero. *lepidocrocite typed layered structure (*Pmmn,* #59).

MI and TiO_2II, ending with the anatase phase. Since MI is significantly unstable at the ambient pressure, TiO_2II is the key intermediate between anatase and rutile. Figure 3 also shows that fluorite is just next to anatase and the layered lepidocrocite is close to rutile, both with high barriers at zero-pressure conditions. Our results for the connectivity between the phases are consistent with the experimental observation. By elevating the pressure to 2.5–7 GPa at ambient temperature, both rutile and anatase phases will transform to TiO_2II phase, to MI at 12 Gpa [52, 53]. The metastable fluorite phase can be found at 48 GPa and 1900–2100 K using anatase as a starting material [54] because it is accessible only kinetically, according to figure 3.

As photocatalysis concerns generally the stable phases at the ambient condition, we now pay more attention to the rutile-to-anatase phase transition (R-to-A), which exhibits clear characteristics of diffusionless transformation, the so-called martensitic transformation. The energy profile for R-to-A shown in figure 3 starts from a rutile monoclinic lattice (a = b = 5.51, c = 4.65 Å, $\alpha = \beta = 90°$, $\gamma = 65.61°$), bypasses the intermediate MI phase with a monoclinic lattice (a = 5.04, b = 4.84, c = 4.92 Å, $\alpha = \beta = 90°$, $\gamma = 80.13°$) and TiO_2II orthorhombic lattice (a = 5.58, b = 4.92, c = 4.57 Å, $\alpha = \beta = \gamma = 90°$), and finally ends at an anatase monoclinic lattice (a = 5.55, b = 5.38, c = 5.37 Å, $\alpha = \gamma = 90°$, $\beta = 61.46°$). The overall barrier is 0.84 eV/cell from DFT, related to the highest TS in between the rutile and TiO_2II.

By closely inspecting the atomic structure change during R-to-A, we can identify the habit plane of the phase transition (on which the atoms shift neither upward nor downward from the surface plane). From rutile to TiO_2II (R-to-II), the transition occurs along the rutile [101] direction ((101) is a ridged facet with the dihedral angle being 67.6° from (110); [hkl] direction with respect to the reciprocal space) and the TiO_2II [001] direction, i.e. the orientation relationship being rutile(101)//TiO_2II(001), rutile[010]//TiO_2II[100]. Both rutile(101) and TiO_2II(001) surfaces are corrugated and expose O_{2c} atoms and Ti_{5c}. As shown in figure 4, we found that these planes show surprising compatibility in the atom registration between phases. The phase transition can follow the martensitic transition mechanism.

From anatase to TiO_2II (A-to-II), the transition initiates along the anatase [112] direction ((112) is a stepped facet with

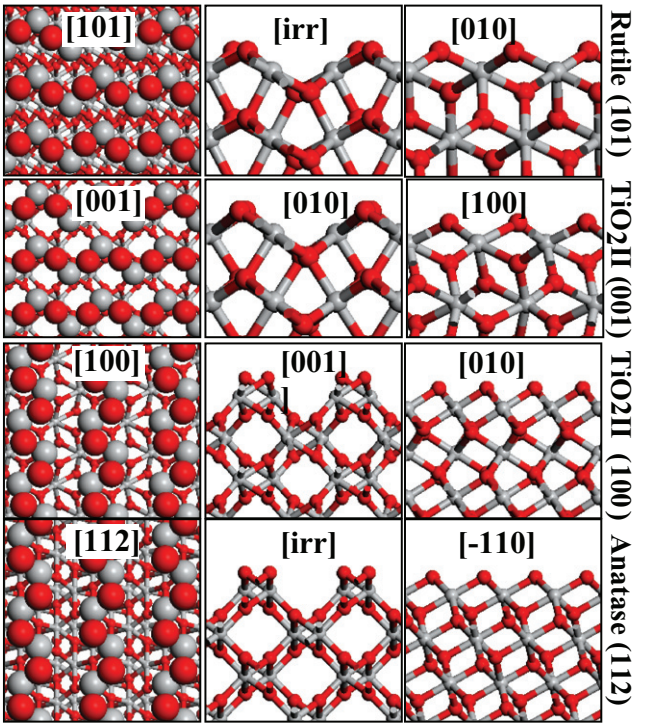

Figure 4. The surface structures of rutile (101), TiO_2II (001) and (100) and anatase (112) at different view angles as labeled in the figure ([hkl] direction with respect to the reciprocal space; irr: irrational direction). Ti atom: grey: O atom: red.

a dihedral angle being 41.2° from anatase (101)), and ends at the TiO_2II [100] direction, i.e. the orientation relationship being anatase(112)//TiO_2II(100), anatase[-110]//TiO_2II[010]. These two surfaces are highly ridged (see figure 4), each ridge being a one-dimensional chain of TiO_2 (also exposing Ti_{5c} and O_{2c} on the top of the chain). Unlike in R-to-II transformation where the high-pressure phase MI (containing Ti_{7c}) appears, the low-coordinated O_{2c} and Ti_{5c} appear at the TS during the A-to-II pathway. The density at the TS is 5.7 percent larger compared to anatase and 5.7 percent lower compared to TiO_2II. It is worth noting that the A-to-II pathway has a comparable but lower barrier (0.70 eV) than that of the R-to-II pathway (0.84 eV). It is implied that TiO_2II as an intermediate phase in between anatase-rutile may be isolated and observed under certain conditions. TiO_2II has been found to grow at the grain boundaries of rutile ores in nature [11], and under lab synthetic conditions, experiments have shown the appearance of the intermediate phase during the anatase to rutile transformation [53].

The R-to-A phase transition mechanism can therefore be summarized as a pathway starting from rutile(101), ending at anatase(112) via the intermediate TiO_2II (001) and (100). These surfaces (habit planes) have close lattice match in general, i.e. all unit cells are rectangular with similar lattice constants (rutile(101): 5.50 × 4.63 Å; TiO_2II(001): 4.56 × 5.57 Å; TiO_2II(100): 4.93 × 5.57 Å and anatase(112): 5.37 × 5.57 Å). The similar surface area, the local coordination and the compatible atomic registration between these surface pairs, rutile/TiO_2II and TiO_2II/anatase, imply the favorable energetics of the three phases in forming the junction. Indeed, by knowing the compatible surfaces, we can readily construct the

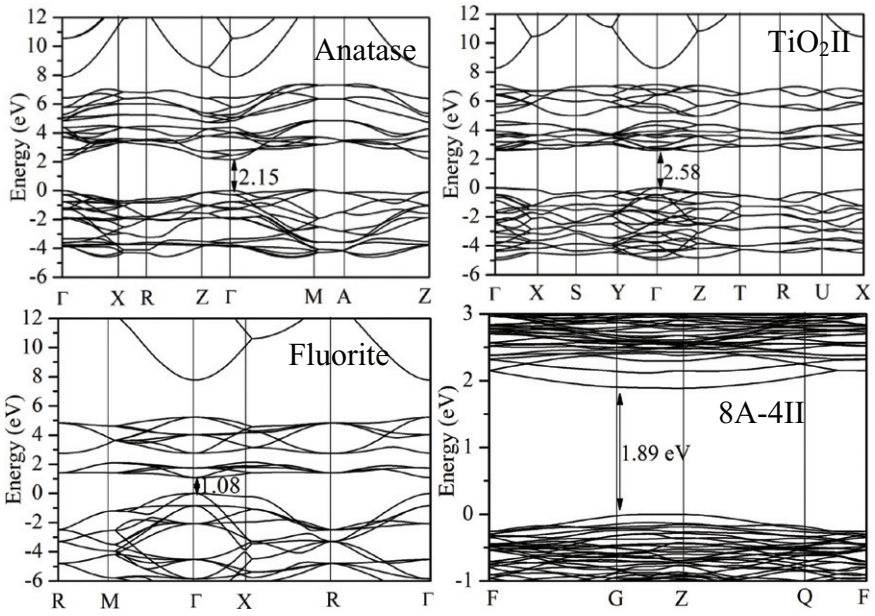

Figure 5. Band structures for selected TiO_2 phases. The anatase-TiO_2II mixed-phase is constructed according to the mechanism illustrated in figure 4: one unit cell of the mixed phase contains 8-layer anatase and 4-layer TiO_2II phase (8A-4II). The energy zero is set as the VBM.

phase junction between the phases by slightly compressing/expanding the lattice relatively (<4%) and shifting the atomic layers (will be illustrated in the next section).

It is worth comparing the R-to-A phase transition mechanism identified here with the knowledge obtained previously. We notice that the stepped anatase {112}, where the phase transformation starts, has been observed during phase transformation by both experiment and MD simulations. Experimentally, Penn *et al* [19] found that by using anatase particles as a seed, the attachment of separated particles occurs mainly via the {112} and {001} surfaces, which is the initial step towards the phase transformation from anatase to rutile. Using high-resolution TEM, they even observed the atomic structure of anatase{112}-twin junction and a few layer of a newly emerged phase freezing in between the {112}-twin junction. The structure of the new phase is not well resolved, often termed as brookite-like phase in literatures. Using a few nano-sized anatase particles as the model, Zhou *et al* [20]. using classical MD simulations also confirmed that {112} twin-like anatase plays a key role in the anatase-rutile transformation.

Our current mechanism of phase transition agrees generally with the previous findings and provides a detailed quantitative description on the lowest energy pathway. While the presence of the intermediate TiO_2II in the mixed rutile-anatase materials has not been confirmed in experiments, we suggest that this might be partly due to the fact that TiO_2II phase can be regarded as a phase of half brookite and half anatase, and it is difficult to distinguish the phase in experiments. On the other hand, TiO_2II being a high-pressure phase is not stable thermodynamically, and kinetically it may also have a short residence time during phase transition because the barriers of A-to-II and II-to-R are close.

3.3. Single phase or mixed phases for photocatalysis

It is of our interest to examine the photoactivity of the identified TiO_2 phases. While a number of factors may influence the photoactivity of material, such as the band gap, the local surface structure, and even the spatial charge separation ability of material [55–57], here we will focus on the band gap of the TiO_2 phases, which is a key measure for the optical properties of material. Because of the large band gap of the abundant TiO_2 phases (> 3 eV for rutile and anatase), it is desirable to identify new materials with narrower band gap allowing the visible light adsorption.

It should be mentioned that the current DFT functional such as PBE tends to underestimate the band gap of TiO_2. For example, the band gap of rutile measured in experiment is ~3.0 eV, while our DFT calculated value is only 1.79 eV. Therefore, it is perhaps more appropriate to compare the band gap relatively between different phases. Indeed, it is known in experiments that the band gap of anatase is ~3.2 eV, 0.2 eV larger than rutile, and consistently the relative band gap of anatase is calculated to be 0.36 eV from DFT (PBE functional). We have also examined the relative band gap of anatase using hybrid DFT calculations at HSE06 functional in CP2K/QUICKSTEP [58] package, which produces a value of 0.42 eV, indicating the DFT at the level of PBE functional is accurate enough for assessing the relative band gap (as also found previously in nanocrystals [55]). In figure 5, we have shown the calculated band structure for selected phases using DFT (PBE) and the relative band gap (ΔEg) with respect to the rutile phase have been listed in table 1.

From the calculated band structure, we found that there are only three phases, namely, #110, pyrite and fluorite that have a band gap smaller than the rutile phase. The new phase #110 has a band gap of 0.29 eV less than the rutile. The high-pressure phase fluorite has a band gap of 0.71 eV less than the rutile, indicating this phase has much improved visible light adsorption ability. Unfortunately, all three phases are very unstable at the ambient pressure. The #110 phase is the most stable among the three phases, but it is already at least 0.513 eV per TiO_2 unit less stable than rutile phase. These results imply that

while it might be difficult to synthesize these pure phase TiO_2 materials in a large quantity at the ambient condition due to the thermodynamics, the growth of a thin-layer TiO_2 structure of these interesting phases may still be kinetically feasible.

On the other hand, the band structure of a mixed phase, anatase-TiO_2II, does show an unexpected band structure feature. This mixed phase can be constructed by gluing the two phases together using the orientation relationship of phase transition mechanism previously discovered. We studied one such an example of a mixed phase with one unit cell containing 8-layer anatase and 4-layer TiO_2II phase (8A-4II, see figure 5). We notice that the band gap of anatase and TiO_2II are both larger than rutile phase from DFT by at least 0.36 eV (see table 1). However, quite unexpectedly, the mixing of the two phases yields a new material with the band gap being smaller than both parent phases, and is only 0.1 eV larger than rutile. Energetically, this mixed phase is also very stable, which is only 0.06 eV per TiO_2 unit less stable than anatase. Because of the natural phase separation in the mixed phase, it is expected that the photocatalytic performance can be improved due to the decreased probability of electron-hole pair recombination. These indicate that the anatase-TiO_2II mixed phase is thermodynamically stable and may have an improved photoactivity compared to the parent phases, considering that the ratio of the phases can be further tuned. Our results provide one plausible explanation for the recent observation that the TiO_2 composites have higher photoactivity than single phases [59, 60]. Further studies are continued in the group to examine the photoactivity of mixed phases.

4. Conclusion

This work represents a bottom–up attempt to search for new phases of TiO_2 via SSW-crystal global optimization method. A database of TiO_2 phases is established by combining SSW-crystal with the Wang-Landau method to explore the PES and five new phases are identified. The geometrical structure and electronic structure are analyzed. For the stable phases at the low pressure, the lowest energy phase transition pathways are then determined by using the SSW-crystal pathway sampling and the variable-cell DESW method for TS location.

The high-pressure TiO_2II phase is found to be the key intermediate between the two most abundant phases, rutile and anatase. The transition pathway initiates from rutile(101), ends at anatase(112) via intermediate TiO_2II(001) and TiO_2II(100) surfaces. These habit planes, rutile(101)/TiO_2II(001) and TiO_2(100)/anatase(112), are corrugated and exhibit closely matched lattices, the same atomic coordination, and the similar atomic registration.

The band structures of all the phases are calculated, showing that three phases—namely, #110, pyrite, and fluorite—have the band gap narrower than rutile phase. However, theses phases are much more unstable at the ambient-pressure condition than rutile. On the other hand, one mixed phase—i.e. the anatase mixed with TiO_2II phase—is examined and found to exhibit good stability and unexpected electronic structure property. The band gap of the mixed phase is narrower than both parent phases, which approaches to that of rutile. Our results suggest that the mixed phase of TiO_2 with tunable composition could be an exciting new area to explore for the design of photocatalysts.

Acknowledgements

We acknowledge the National Science Foundation of China (21173051, 21361130019), 973 program (2011CB808500, 2013CB834603), Science and Technology Commission of Shanghai Municipality (08DZ2270500), and Program for Professor of Special Appointment (Eastern Scholar) at 676 Shanghai Institute of Higher Learning for financial support.

References

[1] Fujishima A and Honda K 1972 *Nature* **238** 37
[2] Nozik A J 1975 *Nature* **257** 383
[3] Zou Z G, Ye J H, Sayama K and Arakawa H 2001 *Nature* **414** 625
[4] Vittadini A, Selloni A, Rotzinger F P and Grätzel M 1998 *Phys. Rev. Lett.* **81** 2954
[5] Schaub R, Thostrup P, Lopez N, Laegsgaard E, Stensgaard I, Norskov J K and Besenbacher F 2001 *Phys. Rev. Lett.* **87** 266104
[6] Xu M C, Gao Y K, Moreno E M, Kunst M, Muhler M, Wang Y M, Idriss H and Woll C 2011 *Phys. Rev. Lett.* **106** 138302
[7] Zhao W-N and Liu Z-P 2014 *Chem. Sci.* **5** 2256
[8] Li Y F, Liu Z P, Liu L L and Gao W G 2010 *J. Am. Chem. Soc.* **132** 13008
[9] Chen J, Li Y-F, Sit P and Selloni A 2013 *J. Am. Chem. Soc.* **135** 18774
[10] El Goresy A, Dubrovinsky L, Gillet P, Graup G and Chen M 2010 *Am. Mineral.* **95** 892
[11] El Goresy A, Chen M, Gillet P, Dubrovinsky L, Graup G and Ahuja R 2001 *Earth Planet. Sci. Lett.* **192** 485
[12] Bickley R I, Gonzalez-Carreno T, Lees J S, Palmisano L and Tilley R J D 1991 *J. Solid State Chem.* **92** 178
[13] Ohno T, Sarukawa K, Tokieda K and Matsumura M 2001 *J. Catal.* **203** 82
[14] Zhang J, Xu Q, Feng Z, Li M and Li C 2008 *Angew. Chem.-Int. Edit.* **47** 1766
[15] Zhang Y, Chen J and Li X 2010 *Catal. Lett.* **139** 129
[16] Ma Y, Xu Q, Chong R F and Li C 2013 *J. Mater. Res.* **28** 394
[17] Linsebigler A L, Lu G and Yates J T 1995 *Chem. Rev.* **95** 735
[18] Penn R L and Banfield J F 1998 *Am. Mineral.* **83** 1077
[19] Penn R L and Banfield J F 1998 *Science* **281** 969
[20] Zhou Y and Fichthorn K A 2012 *J. Phys. Chem.* C **116** 8314
[21] Ricci P C, Carbonaro C M, Stagi L, Salis M, Casu A, Enzo S and Delogu F 2013 *J. Phys. Chem. C* **117** 7850
[22] Shang C and Liu Z P 2013 *J. Chem. Theory Comput.* **9** 1838
[23] Shang C, Zhang X-J and Liu Z-P 2014 *Phys. Chem. Chem. Phys.* **16** 17845–56
[24] Shang C and Liu Z P 2012 *J. Chem. Theory Comput.* **8** 2215
[25] Zhang X-J, Shang C and Liu Z-P 2013 *J. Chem. Theory Comput.* **9** 5745
[26] Shang C and Liu Z-P 2010 *J. Chem. Theory Comput.* **6** 1136
[27] Matsui M and Akaogi M 1991 *Mol. Simul.* **6** 239
[28] Dubrovinskaia N A, Dubrovinsky L S, Ahuja R, Prokopenko V B, Dmitriev V, Weber H P, Osorio-Guillen J M and Johansson B 2001 *Phys. Rev. Lett.* **87** 275501
[29] Payne M C, Teter M P, Allan D C, Arias T A and Joannopoulos J D 1992 *Rev. Mod. Phys.* **64** 1045

[30] Kresse G and Furthmüller J 1996 *Phys. Rev.* B **54** 11169
[31] Vanderbilt D 1990 *Phys. Rev.* B **41** 7892
[32] Perdew J P, Burke K and Ernzerhof M 1997 *Phys. Rev. Lett*. **78** 1396
[33] Perdew J P, Burke K and Ernzerhof M 1996 *Phys. Rev. Lett*. **77** 3865
[34] Soler J M, Artacho E, Gale J D, Garcia A, Junquera J, Ordejon P and Sanchez-Portal D 2002 *J. Phys.: Condens. Matter* **14** 2745
[35] Junquera J, Paz O, Sanchez-Portal D and Artacho E 2001 *Phys. Rev.* B **64** 235111
[36] Anglada E, Soler J M, Junquera J and Artacho E 2002 *Phys. Rev.* B **66** 205101
[37] Wang F G and Landau D P 2001 *Phys. Rev. Lett*. **86** 2050
[38] Caravaca M A, Miño J C, Pérez V J, Casali R A and Ponce C A 2009 *J. Phys.: Condens. Matter* **21** 015501
[39] Muscat J, Swamy V and Harrison N M 2002 *Phys. Rev.* B **65** 224112
[40] Sasaki T, Watanabe M, Hashizume H, Yamada H and Nakazawa H 1996 *J. Am. Chem. Soc*. **118** 8329
[41] Swamy V and Muddle B C 2007 *Phys. Rev. Lett*. **98** 035502
[42] Mei Z-G, Wang Y, Shang S and Liu Z-K 2014 *Comput. Mater. Sci*. **83** 114
[43] Koči L, Kim D Y, Almeida J S d, Mattesini M, Isaev E and Ahuja R 2008 *J. Phys.: Condens. Matter* **20** 345218
[44] Fahmi A, Minot C, Silvi B and Causá M 1993 *Phys. Rev.* B **47** 11717
[45] Labat F, Baranek P, Domain C, Minot C and Adamo C 2007 *J. Chem. Phys*. **126** 154703
[46] Burdett J K, Hughbanks T, Miller G J, Richardson J W and Smith J V 1987 *J. Am. Chem. Soc*. **109** 3639
[47] Mo S-D and Ching W Y 1995 *Phys. Rev.* B **51** 13023
[48] Dewhurst J K and Lowther J E 1996 *Phys. Rev.* B **54** R3673
[49] Glassford K M and Chelikowsky J R 1992 *Phys. Rev.* B **46** 1284
[50] Al-Khatatbeh Y, Lee K K M and Kiefer B 2009 *Phys. Rev.* B **79** 134114
[51] Zhou X-F, Dong X, Qian G-R, Zhang L, Tian Y and Wang H-T 2010 *Phys. Rev. B* **82** 060102
[52] Cai Y Q, Zhang C and Feng Y P 2011 *Phys. Rev.* B **84** 094107
[53] Wu X, Holbig E and Steinle-Neumann G 2010 *J. Phys.: Condens. Matter* **22** 295501
[54] Mattesini M, de Almeida J S, Dubrovinsky L, Dubrovinskaia N, Johansson B and Ahuja R 2004 *Phys. Rev. B* **70** 212101
[55] Li Y-F and Liu Z-P 2011 *J. Am. Chem. Soc*. **133** 15743
[56] Asahi R, Morikawa T, Ohwaki T, Aoki K and Taga Y 2001 *Science* **293** 269
[57] Cernuto G, Masciocchi N, Cervellino A, Colonna G M and Guagliardi A 2011 *J. Am. Chem. Soc*. **133** 3114
[58] VandeVondele J, Krack M, Mohamed F, Parrinello M, Chassaing T and Hutter J 2005 *Comput. Phys. Commun*. **167** 103
[59] Sreethawong T, Suzuki Y and Yoshikawa S 2005 *J. Solid State Chem*. **178** 329
[60] Wang W, Gu M and Jin Y 2003 *Mater. Lett*. **57** 3276